Bayesian inference on a microstructural, hyperelastic model of tendon deformation: Supplementary material
Journal of the Royal Society Interface

James Haughton[1], Jessica E. Forsyth[1], James Casey[1], Simon L. Cotter[1], William J. Parnell[1], and Tom Shearer[1, 2]

[1] *Department of Mathematics, University of Manchester, Manchester M13 9PL, United Kingdom*
[2] *Department of Materials, University of Manchester, Manchester M13 9PL, United Kingdom*

1 SEF derivation

For the reasons stated in the main paper, we assume that the SEF, $W(I_1, I_4)$, is given by

$$W(I_1, I_4) = (1-\phi)W_{\mathrm{NCM}}(I_1) + \phi W_{\mathrm{coll}}(I_4), \tag{1}$$

where ϕ is the collagen volume fraction, $W_{\mathrm{NCM}}(I_1)$ and $W_{\mathrm{coll}}(I_4)$ denote the contributions to the SEF from the non-collagenous matrix (NCM) and collagen fibrils, respectively, I_1 is a strain invariant, and I_4 is the square of the stretch in the direction of the collagen fibrils. As an individual fibril is slack when crimped and obeys Hooke's law when it is taut, the non-dimensional stretch experienced by a fibril, λ_{fib}, in terms of the recruitment stretch, λ_r, at a macroscale stretch λ is

$$\lambda_{\mathrm{fib}}(\lambda, \lambda_r) = \begin{cases} 1, & \lambda < \lambda_r, \\ \frac{\lambda}{\lambda_r}, & \lambda \geqslant \lambda_r. \end{cases} \tag{2}$$

By (2) and the assumptions of the model, the stress in a fibril, $\sigma_{\mathrm{fib}}(\lambda, \lambda_r)$, is

$$\sigma_{\mathrm{fib}}(\lambda, \lambda_r) = E e_{\mathrm{fib}} = \begin{cases} 0, & \lambda < \lambda_r, \\ E\frac{(\lambda-\lambda_r)}{\lambda_r}, & \lambda \geqslant \lambda_r, \end{cases} \tag{3}$$

where E is the Young's modulus of the fibril and $e_{\mathrm{fib}} = \lambda_{\mathrm{fib}} - 1$ is the engineering strain experienced by the fibril. In order to calculate the total stress acting on the collagen fibrils, we must assign a distribution function to model the different recruitment stretches amongst the collagen fibrils. Consequently, $\sigma_F(\lambda)$, the total stress acting on the fibrils, is

$$\sigma_F(\lambda) = \int_0^{\lambda} \sigma_{\mathrm{fib}}(\lambda, \lambda_r) f(\lambda_r) \mathrm{d}\lambda_r, \tag{4}$$

where $f(\lambda_r)$ denotes the recruitment-stretch distribution function.

1.1 General triangular distribution

The probability density function (PDF) for the general triangular distribution is given by

$$f(\lambda_r) = \begin{cases} 0, & \lambda_r < a, \\ \frac{2(\lambda_r - a)}{(b-a)(c-a)}, & a \leqslant \lambda_r \leqslant c, \\ \frac{2(b-\lambda_r)}{(b-a)(b-c)}, & c < \lambda_r \leqslant b, \\ 0, & \lambda_r > b, \end{cases} \tag{5}$$

where a, b, and c are the minimal, maximal, and modal recruitment stretches, respectively. Substituting (3) and (5) into (4), gives

$$\sigma_F(\lambda) = E(A(\lambda) + B(\lambda)\lambda + C(\lambda)\lambda^2 + D(\lambda)\lambda\log\lambda), \tag{6}$$

where $A(\lambda)$, $B(\lambda)$, $C(\lambda)$, and $D(\lambda)$ are piecewise constants that possess the same boundaries as $f(\lambda_r)$ in (5). As the stretch in the direction of the fibrils is λ, then $I_4 = \lambda^2$. Rewriting (6) in terms of I_4, we obtain

$$\sigma_F(I_4) = E\left(A(I_4) + B(I_4)\sqrt{I_4} + C(I_4)I_4 + \frac{D(I_4)}{2}\sqrt{I_4}\ln I_4\right), \tag{7}$$

where

$$A(I_4) = \begin{cases} 0, & I_4 < a^2, \\ -\frac{a^2}{(b-a)(c-a)}, & a^2 \leqslant I_4 \leqslant c^2, \\ \frac{c^2}{(c-a)(b-c)} - \frac{a^2}{(b-a)(c-a)}, & c^2 < I_4 \leqslant b^2, \\ -1, & I_4 > b^2, \end{cases} \tag{8}$$

$$B(I_4) = \begin{cases} 0, & I_4 < a^2, \\ \frac{2a\log a}{(b-a)(c-a)}, & a^2 \leqslant I_4 \leqslant c^2, \\ \frac{2a\log a}{(b-a)(c-a)} - \frac{2c\log c}{(c-a)(b-c)}, & c^2 < I_4 \leqslant b^2, \\ \frac{2a\log a}{(b-a)(c-a)} + \frac{2b\log b}{(b-a)(b-c)} - \frac{2c\log c}{(c-a)(b-c)}, & I_4 > b^2, \end{cases} \tag{9}$$

$$C(I_4) = \begin{cases} 0, & I_4 < a^2, \\ \frac{1}{(b-a)(c-a)}, & a^2 \leqslant I_4 \leqslant c^2, \\ -\frac{1}{(b-a)(b-c)}, & c^2 < I_4 \leqslant b^2, \\ 0, & I_4 > b^2, \end{cases} \tag{10}$$

$$D(I_4) = \begin{cases} 0, & I_4 < a^2, \\ -\frac{2a}{(b-a)(c-a)}, & a^2 \leqslant I_4 \leqslant c^2, \\ \frac{2b}{(b-a)(b-c)}, & c^2 < I_4 \leqslant b^2, \\ 0, & I_4 > b^2. \end{cases} \tag{11}$$

From the main paper, in terms of $W(I_1, I_4)$, the Cauchy stress, $\boldsymbol{\sigma}$, is

$$\boldsymbol{\sigma} = -p\mathbf{I} + 2\frac{\partial W}{\partial I_1}\mathbf{B} + 2\frac{\partial W}{\partial I_4}\mathbf{m}\otimes\mathbf{m}, \tag{12}$$

where p is a Lagrange multiplier that accounts for the loss of a degree of freedom that is caused by the assumption of incompressibility, $\mathbf{B}$ is the left Cauchy-Green deformation tensor, and $\mathbf{m}$ is the deformed orientation of the collagen fibrils. By (1) and (12), the fibril contribution to the Cauchy stress, $\boldsymbol{\sigma}_{\text{coll}}$, is

$$\boldsymbol{\sigma}_{\text{coll}} = 2\frac{\partial W_{\text{coll}}(I_4)}{\partial I_4}\mathbf{m}\otimes\mathbf{m}. \tag{13}$$

We can rewrite the right side of (13) in terms of I_4 using the method outlined in [1]. First, we calculate the traction, $\mathbf{t}_{\text{coll}}$, associated with the contribution to the stress from the collagen fibrils that acts on a face normal to the fibrils. Then we calculate the component of $\mathbf{t}_{\text{coll}}$ that acts in the direction of the fibrils. We find

$$\left(\boldsymbol{\sigma}_{\text{coll}}\cdot\left(\frac{\mathbf{m}}{|\mathbf{m}|}\right)\right)\cdot\frac{\mathbf{m}}{|\mathbf{m}|} = \frac{\mathbf{t}_{\text{coll}}\cdot\mathbf{m}}{|\mathbf{m}|} = \left(2\frac{\partial W_{\text{coll}}(I_4)}{\partial I_4}|\mathbf{m}|\mathbf{m}\right)\cdot\frac{\mathbf{m}}{|\mathbf{m}|} = 2I_4\frac{\partial W_{\text{coll}}(I_4)}{\partial I_4}. \tag{14}$$

By (7) and (14),

$$2I_4\frac{\partial W_{\text{coll}}(I_4)}{\partial I_4} = E\left(A(I_4) + B(I_4)\sqrt{I_4} + C(I_4)I_4 + \frac{D(I_4)}{2}\sqrt{I_4}\ln I_4\right). \tag{15}$$

Consequently,

$$W_{\text{coll}}(I_4) = E\left(\frac{A(I_4)}{2}\log I_4 + (B(I_4) - D(I_4))\sqrt{I_4} + \frac{C(I_4)}{2}I_4 + \frac{D(I_4)}{2}\sqrt{I_4}\log I_4 + G(I_4)\right), \tag{16}$$

where $G(I_4)$ ensures the continuity of $W_{\text{coll}}(I_4)$ across each boundary of $A(I_4)$—$D(I_4)$, and is equal to

$$G(I_4) = \begin{cases} 0, & I_4 < a^2, \\ \frac{a^2 \log a}{(b-a)(c-a)} - \frac{5a^2}{2(b-a)(c-a)}, & a^2 \leqslant I_4 \leqslant c^2, \\ \frac{a^2 \log a}{(b-a)(c-a)} - \frac{c^2 \log c}{(c-a)(b-c)} - \frac{5a^2}{2(b-a)(c-a)} + \frac{5c^2}{2(b-c)(c-a)}, & c^2 \leqslant I_4 \leqslant b^2, \\ \frac{a^2 \log a}{(b-a)(c-a)} - \frac{c^2 \log c}{(c-a)(b-c)} + \frac{b^2 \log b}{(b-c)(b-a)} - \frac{5a^2}{2(b-a)(c-a)} + \frac{5c^2}{2(b-c)(c-a)} - \frac{5b^2}{2(b-a)(b-c)}, & I_4 > b^2. \end{cases} \tag{17}$$

We assume a neo-Hookean contribution to the SEF from the NCM. Therefore, the new SEF is given by

$$\begin{aligned} W(I_1, I_4) = {} & (1-\phi)\frac{\mu}{2}(I_1 - 3) \\ & + \phi E\bigg(\frac{A(I_4)}{2}\log I_4 + (B(I_4) - D(I_4))\sqrt{I_4} + \frac{C(I_4)}{2}I_4 + \frac{D(I_4)}{2}\sqrt{I_4}\log I_4 + G(I_4)\bigg). \end{aligned} \tag{18}$$

1.2 Symmetric triangular distribution

We can restrict the triangular distribution to be symmetric. That is, we set the mode, c, to be equal to $\frac{a+b}{2}$. Therefore, (5) becomes

$$f(\lambda_r) = \begin{cases} 0, & \lambda_r < a, \\ \frac{4(\lambda_r - a)}{(b-a)^2}, & a \leqslant \lambda_r \leqslant \frac{a+b}{2}, \\ \frac{4(b-\lambda_r)}{(b-a)^2}, & \frac{a+b}{2} < \lambda_r \leqslant b, \\ 0, & \lambda_r > b. \end{cases} \tag{19}$$

We can insert (3) and (19) into (4) to calculate the total contribution to the stress from the fibrils. Similar to (6), we find that

$$\sigma^*(I_4) = E\left(A^*(I_4) + B^*(I_4)\sqrt{I_4} + C^*(I_4)I_4 + \frac{D^*(I_4)}{2}\sqrt{I_4}\log I_4\right), \tag{20}$$

where $I_4 = \lambda^2$ and

$$A^*(I_4) = \begin{cases} 0, & I_4 < a^2, \\ -\frac{2a^2}{(b-a)^2}, & a^2 \leqslant I_4 \leqslant \left(\frac{a+b}{2}\right)^2, \\ \frac{(b^2 - a^2 + 2ab)}{(b-a)^2}, & \left(\frac{a+b}{2}\right)^2 < I_4 \leqslant b^2, \\ -1, & I_4 > b^2, \end{cases} \tag{21}$$

$$B^*(I_4) = \begin{cases} 0, & I_4 < a^2, \\ \frac{4a\log a}{(b-a)^2}, & a^2 \leqslant I_4 \leqslant \left(\frac{a+b}{2}\right)^2, \\ \frac{4a\log a}{(b-a)^2} - \frac{4(b+a)}{(b-a)^2}\log\left(\frac{a+b}{2}\right), & \left(\frac{a+b}{2}\right)^2 < I_4 \leqslant b^2, \\ \frac{4a\log a}{(b-a)^2} + \frac{4b\log b}{(b-a)^2} - \frac{4(b+a)}{(b-a)^2}\log\left(\frac{a+b}{2}\right), & I_4 > b^2, \end{cases} \tag{22}$$

$$C^*(I_4) = \begin{cases} 0, & I_4 < a^2, \\ \frac{2}{(b-a)^2}, & a^2 \leqslant I_4 \leqslant \left(\frac{a+b}{2}\right)^2, \\ -\frac{2}{(b-a)^2}, & \left(\frac{a+b}{2}\right)^2 < I_4 \leqslant b^2, \\ 0, & I_4 > b^2, \end{cases} \tag{23}$$

$$D^*(I_4) = \begin{cases} 0, & I_4 < a^2, \\ -\frac{4a}{(b-a)^2}, & a^2 \leqslant I_4 \leqslant \left(\frac{a+b}{2}\right)^2, \\ \frac{4b}{(b-a)^2}, & \left(\frac{a+b}{2}\right)^2 < I_4 \leqslant b^2, \\ 0, & I_4 > b^2. \end{cases} \tag{24}$$

By (20) and (14),

$$W^*_{\text{coll}}(I_4) = E\left(\frac{A^*(I_4)}{2}\log I_4 + (B^*(I_4) - D^*(I_4))\sqrt{I_4} + \frac{C^*(I_4)}{2}I_4 + \frac{D^*(I_4)}{2}\sqrt{I_4}\log I_4 + G^*(I_4)\right), \tag{25}$$

where G^* is an integration constant that ensures the continuity of $W^*_{\text{coll}}(I_4)$ at each of the boundaries defined in $A^*(I_4)$—$D^*(I_4)$, and is given by

$$G^*(I_4) = \begin{cases} 0, & I_4 < a^2, \\ \frac{2a^2\log a}{(b-a)^2} - \frac{5a^2}{(b-a)^2}, & a^2 \leqslant I_4 \leqslant \left(\frac{a+b}{2}\right)^2, \\ \frac{2a^2\log a}{(b-a)^2} - \frac{(a+b)^2\log\left(\frac{a+b}{2}\right)}{(b-a)^2} - \frac{5a^2}{(b-a)^2} + \frac{5(a+b)^2}{2(b-a)^2}, & \left(\frac{a+b}{2}\right)^2 \leqslant I_4 \leqslant b^2, \\ \frac{2a^2\log a}{(b-a)^2} - \frac{(a+b)^2\log\left(\frac{a+b}{2}\right)}{(b-a)^2} + \frac{2b^2\log b}{(b-a)^2} - \frac{5a^2}{(b-a)^2} + \frac{5(a+b)^2}{2(b-a)^2} - \frac{5b^2}{(b-a)^2}, & I_4 > b^2. \end{cases} \tag{26}$$

Again, we choose to model the contribution to the SEF from the non-collagenous matrix with a neo-Hookean model. Therefore,

$$\begin{aligned} W^*(I_1, I_4) &= (1-\phi)\frac{\mu}{2}(I_1 - 3) \\ &\quad + \phi E\left(\frac{A^*(I_4)}{2}\log I_4 + (B^*(I_4) - D^*(I_4))\sqrt{I_4} + \frac{C^*(I_4)}{2}I_4 + \frac{D^*(I_4)}{2}\sqrt{I_4}\log I_4 + G^*(I_4)\right). \end{aligned} \tag{27}$$

2 Mathematica Plots

In the main paper, we analyse the quality of fit achieved by several models of soft tissue deformation to two sets of stress-strain data taken from tendon samples by Goh *et al.*, designated in the paper as t5c and t6b, and two sets of mechanical equine tendon data collected by Screen *et al*, designated as superficial digital flexor tendon (SDFT) and common digital extensor tendon (CDET). These fits were obtained using the `NonlinearModelFit` function in Mathematica 12.3.1.0. As mentioned in the main paper, fitting a particular model to any one of the data sets was performed five times in total, with the estimated parameter values at the end of one iteration of the fitting process providing the initial parameter estimates for the following iteration. A couple of the fits achieved are shown in the main paper. In this supplementary material, however, we provide the fits to each data set from all four of the models that we fit to the data sets. In particular, we plot the fits obtained from the fifth iteration of fitting the models to the data. The fits to the four data sets for the HGO model and the microstructural tendon model are provided in Figure 1 and Figure 2, respectively. For the ST and GT models, the fits are in Figure 3 and Figure 4, respectively.

3 Hierarchical Bayes and the posterior predictive

In the main paper, we model the noise inherent in the problem with a Gaussian distribution of mean zero and covariance matrix $\sigma^2\mathbf{I}_d$, where d is the length of the data. Therefore, we obtain the following expression for the likelihood function, $L(\mathbf{y}|\boldsymbol{\theta}, \sigma^2)$:

$$\begin{aligned} L(\mathbf{y}|\boldsymbol{\theta}, \sigma^2) &= \prod_{i=1}^{d} \frac{1}{\sqrt{2\pi\sigma^2}} \exp\left(-\frac{1}{2\sigma^2}(y_i - M(\boldsymbol{\theta})_i)^2\right), \\ &= \left(\frac{1}{2\pi\sigma^2}\right)^{\frac{d}{2}} \exp\left(-\frac{1}{2\sigma^2}\sum_{i=1}^{d}(y_i - M(\boldsymbol{\theta})_i)^2\right), \end{aligned} \tag{28}$$

where $\mathbf{y}$ is the experimental data, $\boldsymbol{\theta}$ is the parameter vector, and $\mathbf{M}(\boldsymbol{\theta})$ is the predicted stress-strain vector. In (28), $L(\mathbf{y}|\boldsymbol{\theta}, \sigma^2)$ possesses the same form for $\mathbf{y}$ as a Gaussian distribution with mean $\mathbf{M}(\boldsymbol{\theta})$ and variance $\sigma^2\mathbf{I}_d$.

To find the posterior distribution, up to a normalisation constant, we multiply the likelihood function in (28) by the prior distributions of the model's parameters, $\boldsymbol{\theta}$ and σ^2. *A priori*, we assume that the parameters are independent of one another, and so the joint prior is just a product of the parameters' individual priors. That is,

$$\pi_0(\boldsymbol{\theta}, \sigma^2) = \pi_0(\theta_1)\cdots\pi_0(\theta_h)\pi_0(\sigma^2), \tag{29}$$

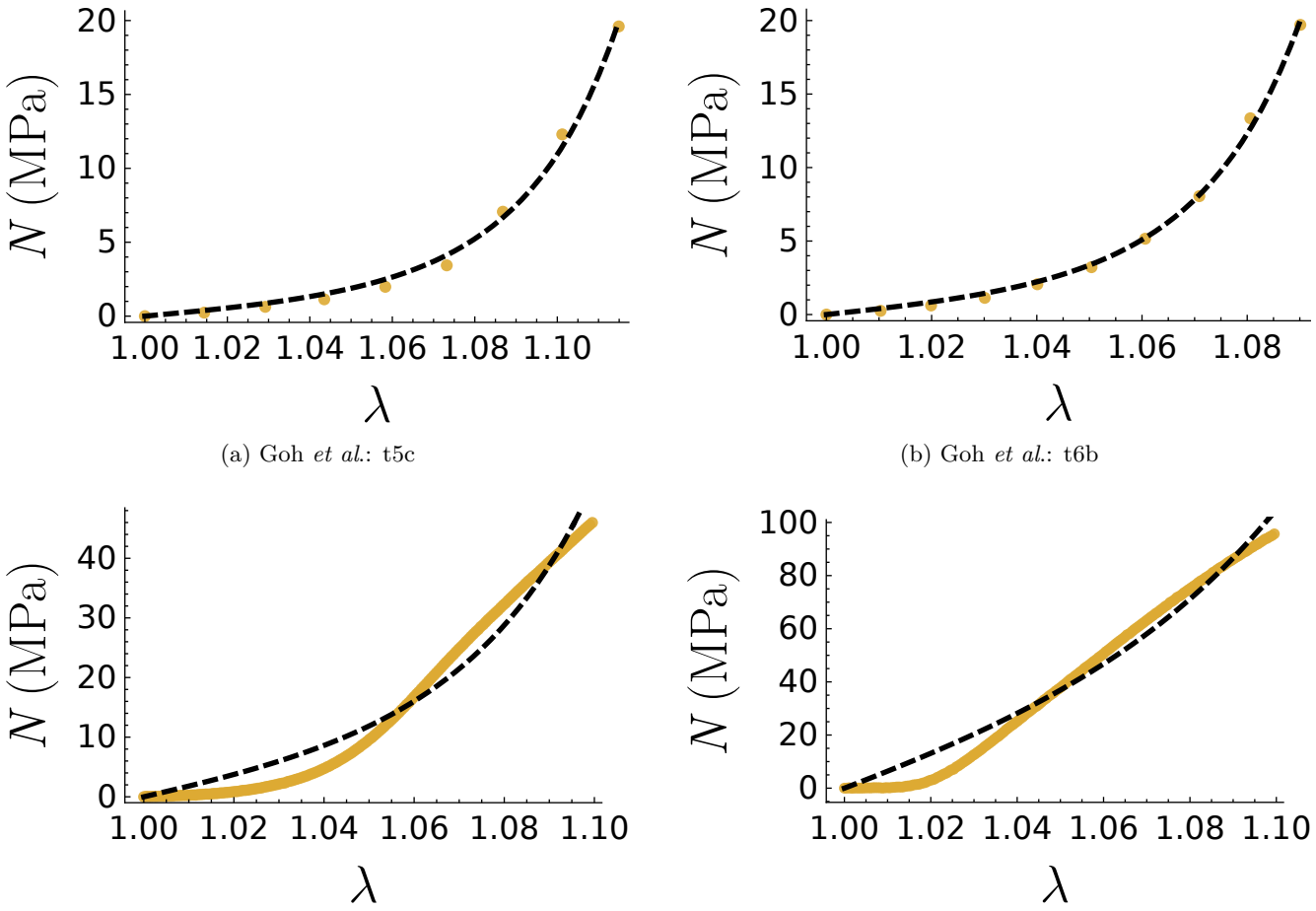

(a) Goh *et al.*: t5c

(b) Goh *et al.*: t6b

(c) Screen *et al.*: SDFT

(d) Screen *et al.*: CDET

Figure 1: Closest fits (black, dashed lines) to the experimental tendon stress-strain data (yellow circles) using the HGO model.

where $\pi_0(*)$ represents the prior distribution of $*$ and h denotes the length of $\boldsymbol{\theta}$. With (29) and by Bayes' rule, the posterior distribution, $\pi(\boldsymbol{\theta}, \sigma^2|\mathbf{y})$, is

$$\pi(\boldsymbol{\theta}, \sigma^2|\mathbf{y}) \propto L(\mathbf{y}|\boldsymbol{\theta}, \sigma^2)\pi_0(\theta_1)\cdots\pi_0(\theta_h)\pi_0(\sigma^2). \tag{30}$$

To characterise the posterior distribution fully, we must compute the following multi-dimensional integral

$$Z = \int_{\mathbb{R}^h}\int_{\mathbb{R}} L(\mathbf{y}|\boldsymbol{\theta}, \sigma^2)\pi_0(\theta_1)\cdots\pi_0(\theta_h)\pi_0(\sigma^2)\mathrm{d}\sigma^2\mathrm{d}\boldsymbol{\theta}. \tag{31}$$

To compute Z as defined in (31) would be impractical due to the non-linear nature of the likelihood; however, because of the form of the likelihood in (28), we can use a technique employed in the literature [2] to simplify the problem by integrating the posterior with respect to σ^2. To enable this integration to be performed, we make an appropriate choice of $\pi_0(\sigma^2)$, known as a conjugate prior, which ensures that $L(\mathbf{y}|\boldsymbol{\theta}, \sigma^2)\pi_0(\sigma^2)$ retains the same functional form as the conjugate prior itself. We choose the conjugate prior, $\pi_0(\sigma^2)$, to be an inverse-gamma distribution, which possesses the following PDF:

$$\pi_0(\sigma^2|\alpha_\sigma, \beta_\sigma) = \frac{\beta_\sigma^{\alpha_\sigma}}{\Gamma(\alpha_\sigma)}(\sigma^2)^{-\alpha_\sigma-1}\exp\left(-\frac{\beta_\sigma}{\sigma^2}\right), \tag{32}$$

where $\Gamma(*)$ represents the Gamma function of $*$, and α_σ and β_σ are distribution parameters of the inverse-gamma distribution, which correspond to the shape and scale of the PDF, respectively. The parameters α_σ and β_σ are hyperparameters. That is, they are not parameters that we estimate the value of in the Random Walk Metropolis

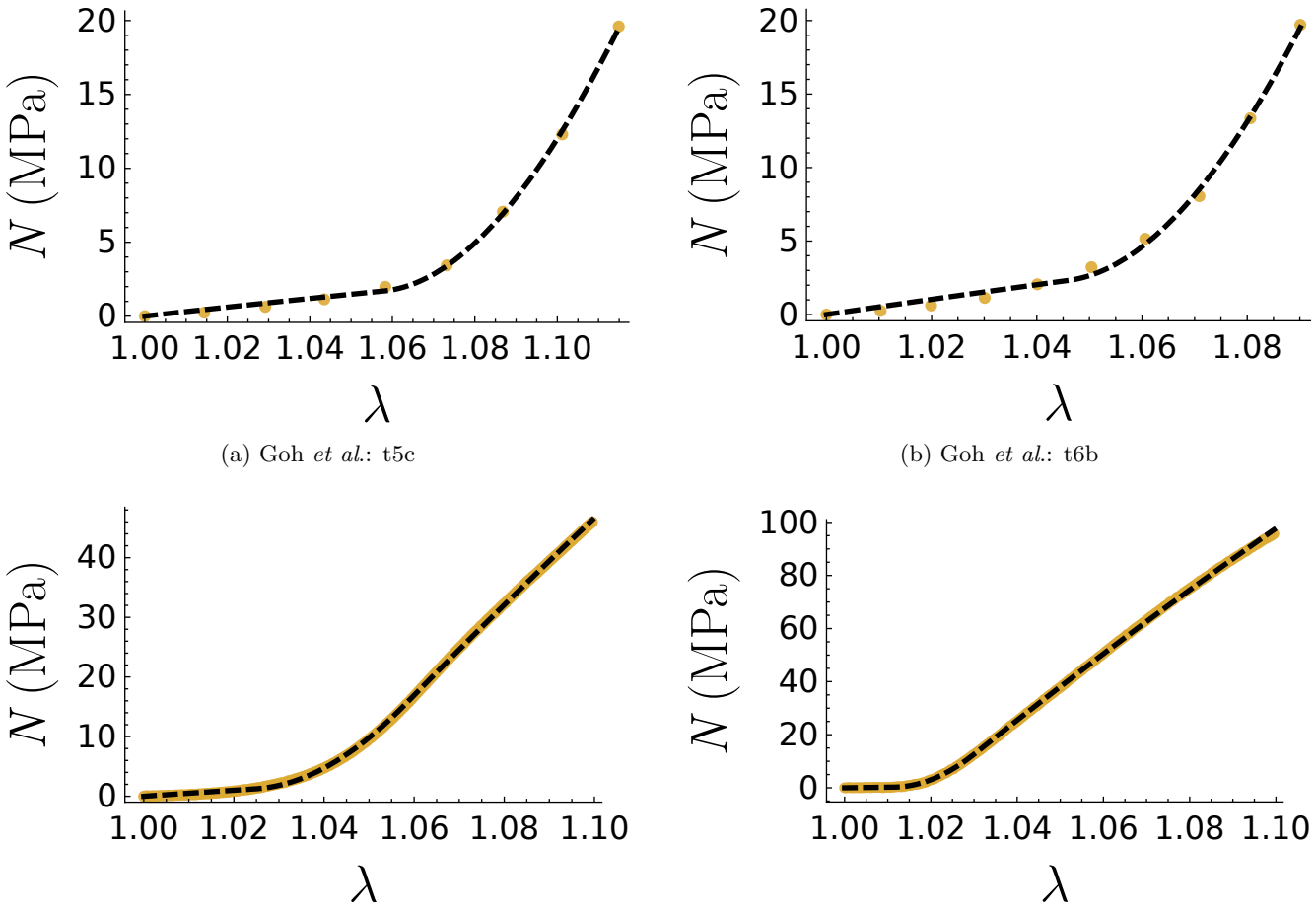

(a) Goh *et al.*: t5c

(b) Goh *et al.*: t6b

(c) Screen *et al.*: SDFT

(d) Screen *et al.*: CDET

Figure 2: Closest fits (black, dashed lines) to the experimental tendon stress-strain data (yellow circles) using the modified microstructural tendon model.

(RWM) algorithm. Instead, we choose the values of the hyperparameters, which are constant in the integration with respect to σ^2. Consequently, by (28) and (32),

$$\begin{aligned}\int_0^\infty L(\mathbf{y}|\boldsymbol{\theta},\sigma^2)\pi_0(\sigma^2)\mathrm{d}\sigma^2 &= \int_0^\infty \frac{\beta_\sigma^{\alpha_\sigma}\cdot(\sigma^2)^{-\frac{d}{2}}}{(2\pi)^{\frac{d}{2}}\Gamma(\alpha_\sigma)}\exp\left(-\frac{\Delta^2}{2\sigma^2}\right)(\sigma^2)^{-\alpha_\sigma-1}\exp\left(-\frac{\beta_\sigma}{\sigma^2}\right)\mathrm{d}\sigma^2,\\ &\propto \int_0^\infty (\sigma^2)^{-\left(\frac{d}{2}+\alpha_\sigma\right)-1}\exp\left(-\frac{(\frac{\Delta^2}{2}+\beta_\sigma)}{\sigma^2}\right)\mathrm{d}\sigma^2,\end{aligned} \tag{33}$$

where $\Delta^2 = \sum_{i=1}^d (y_i - M(\boldsymbol{\theta})_i)^2$. By choosing an inverse-gamma prior for σ^2, $L(\mathbf{y}|\boldsymbol{\theta},\sigma^2)\pi_0(\sigma^2)$ shares the same functional form as $\pi_0(\sigma^2)$, (32) and (33), with α_σ replaced by $\frac{d}{2}+\alpha_\sigma$, and β_σ replaced by $\frac{\Delta^2}{2}+\beta_\sigma$. Therefore, when we integrate $L(\mathbf{y}|\boldsymbol{\theta},\sigma^2)\pi_0(\sigma^2)$ with respect to σ^2, we obtain

$$\int_0^\infty (\sigma^2)^{-\left(\frac{d}{2}+\alpha_\sigma\right)-1}\exp\left(-\frac{(\frac{\Delta^2}{2}+\beta_\sigma)}{\sigma^2}\right)\mathrm{d}\sigma^2 = \frac{\Gamma(\frac{d}{2}+\alpha_\sigma)}{(\frac{\Delta^2}{2}+\beta_\sigma)^{\frac{d}{2}+\alpha_\sigma}}. \tag{34}$$

By (28), (32) and (34),

$$L^{(\sigma^2)}(\mathbf{y}|\boldsymbol{\theta}) = \frac{\beta_\sigma^{\alpha_\sigma}\Gamma(\frac{d}{2}+\alpha_\sigma)}{(2\pi)^{\frac{d}{2}}\Gamma(\alpha_\sigma)(\frac{\Delta^2}{2}+\beta_\sigma)^{\frac{d}{2}+\alpha_\sigma}}. \tag{35}$$

The quantity $L^{(\sigma^2)}(\mathbf{y}|\boldsymbol{\theta})$ is known as the posterior-predictive.

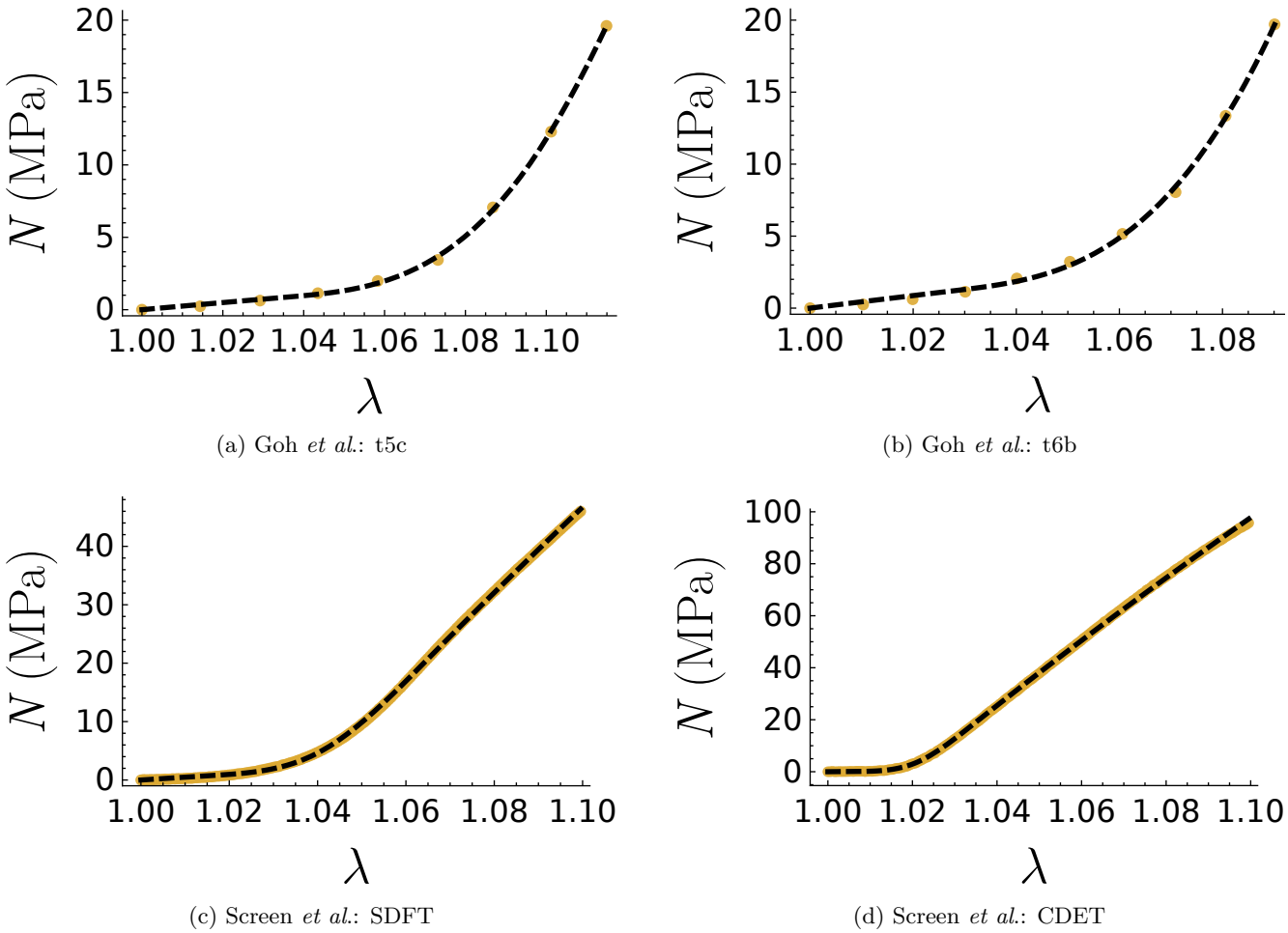

(a) Goh *et al.*: t5c

(b) Goh *et al.*: t6b

(c) Screen *et al.*: SDFT

(d) Screen *et al.*: CDET

Figure 3: Closest fits (black, dashed lines) to the experimental tendon stress-strain data (yellow circles) using the ST model.

For a t-random vector $\mathbf{x}$ of length d, the PDF for the Student's t distribution with mean $\boldsymbol{\mu}$, symmetric matrix parameter $\boldsymbol{\Sigma}$, and ν degrees of freedom is

$$\mathrm{t}_\nu(\mathbf{x};\boldsymbol{\mu},\boldsymbol{\Sigma}) = \frac{\Gamma\left(\frac{\nu+d}{2}\right)}{\Gamma\left(\frac{\nu}{2}\right)} \frac{1}{(\nu\pi)^{\frac{d}{2}}} \frac{1}{\sqrt{\det(\boldsymbol{\Sigma})}} \left(1 + \frac{1}{\nu}(\mathbf{x}-\boldsymbol{\mu})^T\boldsymbol{\Sigma}^{-1}(\mathbf{x}-\boldsymbol{\mu})\right)^{-\frac{d+\nu}{2}}. \tag{36}$$

If we set $\mu = \mathbf{M}(\boldsymbol{\theta})$, $\boldsymbol{\Sigma} = \frac{\beta_\sigma}{\alpha_\sigma}\mathbf{I}_d$, $\mathbf{x} = \mathbf{y}$, and $\nu = 2\alpha_\sigma$, then we eventually recover (35). To show this, we start with (36) and make the aforementioned substitutions,

$$\begin{aligned}
\mathrm{t}\left(\mathbf{y};\mathbf{M}(\boldsymbol{\theta}),\frac{\beta_\sigma}{\alpha_\sigma}\mathbf{I}_d,2\alpha_\sigma\right) &= \frac{\Gamma\left(\alpha_\sigma+\frac{d}{2}\right)}{\Gamma\left(\alpha_\sigma\right)} \frac{1}{(2\alpha_\sigma\pi)^{\frac{d}{2}}} \frac{1}{\sqrt{\frac{\beta_\sigma^d}{\alpha_\sigma^d}}} \left(1 + \frac{1}{2\alpha_\sigma}(\mathbf{y}-\mathbf{M}(\boldsymbol{\theta}))^{\mathrm{T}}\left(\frac{\beta_\sigma}{\alpha_\sigma}\mathbf{I}_d\right)^{-1}(\mathbf{y}-\mathbf{M}(\boldsymbol{\theta}))\right)^{-\omega}, \\
&= \frac{\Gamma(\alpha_\sigma+\frac{d}{2})}{\Gamma(\alpha_\sigma)} \frac{\alpha_\sigma^{\frac{d}{2}}}{(2\alpha_\sigma\pi)^{\frac{d}{2}}} \frac{1}{\beta_\sigma^{\frac{d}{2}}} \left(1 + \frac{1}{2\beta_\sigma}\sum_{i=1}^{d}(y_i - M(\boldsymbol{\theta})_i)^2\right)^{-\omega}, \\
&= \frac{\Gamma(\alpha_\sigma+\frac{d}{2})}{\Gamma(\alpha_\sigma)} \frac{\beta_\sigma^{\alpha_\sigma}}{(2\pi)^{\frac{d}{2}}} \left(\beta_\sigma + \frac{1}{2}\sum_{i=1}^{d}(y_i - M(\boldsymbol{\theta})_i)^2\right)^{-\omega},
\end{aligned} \tag{37}$$

where $\omega = \frac{d}{2} + \alpha_\sigma$. Therefore, the posterior predictive, $L^{(\sigma^2)}(\mathbf{y}|\boldsymbol{\theta})$, is $\mathrm{t}_{2\alpha_\sigma}(\mathbf{y};\mathbf{M}(\boldsymbol{\theta}),\frac{\beta_\sigma}{\alpha_\sigma}\mathbf{I}_d)$, and, by Bayes' rule,

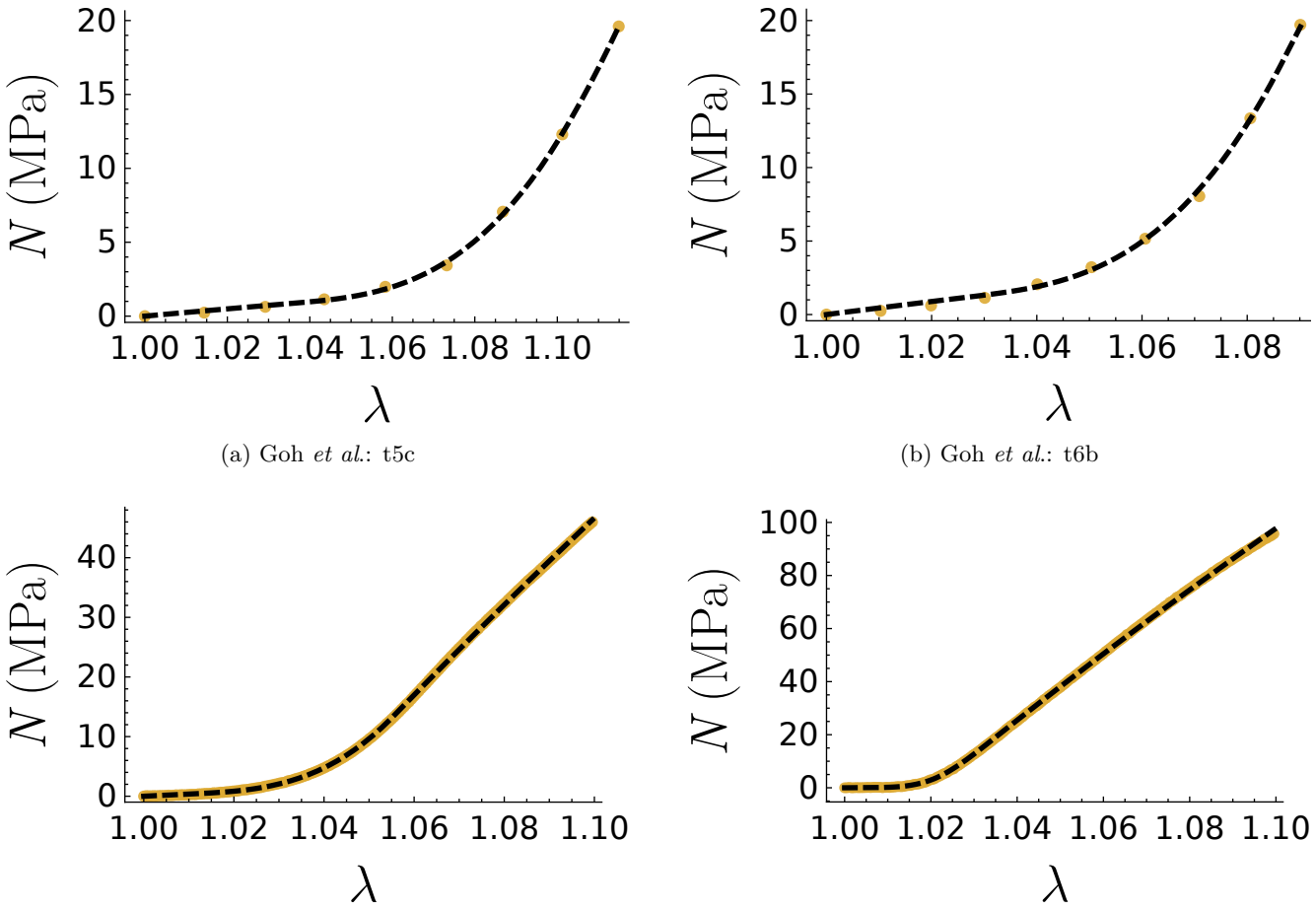

(a) Goh *et al.*: t5c

(b) Goh *et al.*: t6b

(c) Screen *et al.*: SDFT

(d) Screen *et al.*: CDET

Figure 4: Closest fits (black, dashed lines) to the experimental tendon stress-strain data (yellow circles) using the GT model.

$$\begin{aligned}\pi(\boldsymbol{\theta}|\mathbf{y}) &\propto L^{(\sigma^2)}(\mathbf{y}|\boldsymbol{\theta})\pi_0(\boldsymbol{\theta}),\\ &\propto \mathrm{t}_{2\alpha_\sigma}\left(\mathbf{y}; \mathbf{M}(\boldsymbol{\theta}), \frac{\beta_\sigma}{\alpha_\sigma}\mathbf{I}_d\right)\pi_0(\boldsymbol{\theta}).\end{aligned} \tag{38}$$

In order to obtain the exact form of the posterior distribution, we must compute the following integral:

$$Z = \int_{\mathbb{R}^h} L^{(\sigma^2)}(\mathbf{y}|\boldsymbol{\theta})\pi_0(\theta_1)\cdots\pi_0(\theta_h)\mathrm{d}\boldsymbol{\theta}. \tag{39}$$

However, with the form of the posterior predictive and the prior distributions we assign to the model parameters, which are detailed in the main paper, we cannot perform the multi-dimensional integration needed to characterise the posterior distribution exactly. Therefore, we use Markov chain Monte Carlo methods to sample from the distribution instead.

4 Map-induced density

In the main paper, we discuss transforming the unknown parameters in order to sample a set of parameters whose support stretches over the real numbers, thereby matching the support of the proposal distribution. This improves the efficiency of the algorithm and, thus, the quality of our results. Because the transformation between the *target* (untransformed) parameters and the *reference* (transformed) parameter vectors is non-linear, we must account for

the effect that sampling in the reference parameter space has on both the posterior probability for a particular reference vector (and their corresponding values in the target parameter space) and, ultimately, on which proposed vectors are accepted. We must do this when the transformation is non-linear because, in the RWM algorithm, we use a multivariate Gaussian proposal distribution that ensures the probability of moving from a proposed reference parameter vector, $\boldsymbol{\theta}^*$, to the current position of the Markov chains, $\boldsymbol{\theta}_{\text{curr}}$, is the same as moving from $\boldsymbol{\theta}_{\text{curr}}$ to $\boldsymbol{\theta}^*$. However, the probability of moving from the corresponding proposed vector in the target space, $\boldsymbol{\psi}^*$, to $\boldsymbol{\psi}_{\text{curr}}$ may not be the same as the probability of moving from $\boldsymbol{\psi}_{\text{curr}}$ to $\boldsymbol{\psi}^*$. As mentioned in the main paper, we account for this effect by multiplying the posterior probability associated with $\boldsymbol{\psi}$ by the term $|\det D_{T^{-1}}(\boldsymbol{\theta})|$, where $T^{-1}(\boldsymbol{\theta})$ represents the transformation of $\boldsymbol{\theta}$ to $\boldsymbol{\psi}$, $D_{T^{-1}}(\boldsymbol{\theta})$ represents the Jacobian of $T^{-1}(\boldsymbol{\theta})$, and det denotes the determinant of the matrix. Writing the target density with respect to the transformed parameters as $\tilde{\pi}(*)$ and in the original parameter space as $\pi(*)$,

$$\tilde{\pi}(\boldsymbol{\theta}) = \pi(T^{-1}(\boldsymbol{\theta})).|\det D_{T^{-1}}(\boldsymbol{\theta})|. \tag{40}$$

The quantity $\tilde{\pi}(\boldsymbol{\theta})$ is also known as the map-induced density. As defined in the main paper,

$$\boldsymbol{\psi} = \begin{pmatrix} (1-\phi)\mu \\ \phi E \\ a \\ b \end{pmatrix}, \quad T(\boldsymbol{\psi}) = \boldsymbol{\theta} = \begin{pmatrix} \nu \\ \eta \\ \tau \\ \rho \end{pmatrix} = \begin{pmatrix} \log\left((1-\phi)\mu\right) \\ \log\left(\phi E\right) \\ \log\left(a-1\right) \\ \log\left(b-a\right) \end{pmatrix}. \tag{41}$$

Therefore, the transformation T^{-1} is given by

$$T^{-1}(\boldsymbol{\theta}) = \boldsymbol{\psi} = \begin{pmatrix} \exp(\nu) \\ \exp(\eta) \\ \exp(\tau)+1 \\ \exp(\rho)+\exp(\tau)+1 \end{pmatrix}. \tag{42}$$

Therefore, $D_{T^{-1}}(\boldsymbol{\theta})$ is given by

$$D_{T^{-1}}(\boldsymbol{\theta}) = \begin{pmatrix} \exp(\nu) & 0 & 0 & 0 \\ 0 & \exp(\eta) & 0 & 0 \\ 0 & 0 & \exp(\tau) & 0 \\ 0 & 0 & \exp(\tau) & \exp(\rho) \end{pmatrix}. \tag{43}$$

The determinant of the 4×4 matrix $D_{T^{-1}}(\boldsymbol{\theta})$ is thus

$$\det D_{T^{-1}}(\boldsymbol{\theta}) = \exp(\nu+\eta+\tau+\rho). \tag{44}$$

In the RWM algorithm, the acceptance probability involves the evaluation of the target density at the current and proposed states, which, in this instance, is given by the map-induced density

$$\tilde{\pi}(\boldsymbol{\theta}) = \pi(T^{-1}(\boldsymbol{\theta})).\exp(\nu+\eta+\tau+\rho). \tag{45}$$

5 Transformation of the engineering stress using the new parameters

In this section, we rewrite the constitutive equation for the ST model in terms of the transformed parameters, ν, η, τ, and ρ. Respectively, these parameters are the natural logarithms of $(1-\phi)\mu$, ϕE, $a-1$, $b-a$. For a uniaxial stretch along the z-axis, which coincides with the orientation of the collagen fibrils, and assuming traction-free boundary conditions on faces that are not normal to the z-axis, the only non-zero component of the Cauchy stress as defined in (12), σ_{zz}, is

$$\sigma_{zz} = (1-\phi)\mu\left(\lambda^2 - \frac{1}{\lambda}\right) + \phi E(A^*(\lambda) + B^*(\lambda)\lambda + C^*(\lambda)\lambda^2 + D^*(\lambda)\lambda\log\lambda). \tag{46}$$

We can use (21)—(24) and (46) to write σ_{zz} explicitly in terms of λ and the transformed parameters for each region specified in the piecewise constants. As discussed in the main paper, the following equations for σ_{zz} are divided by λ and can then be used in the adaptive RWM algorithm to fit to stress-strain data.

5.1 Region 1

In this region, every collagen fibril is crimped and slack. Only the non-collagenous matrix contributes to the tendon's resistance to the deformation. In terms of the transformed parameters, this region is defined as $\lambda < 1 + \mathrm{e}^{\tau}$ and the Cauchy stress is

$$\sigma_{zz} = \mathrm{e}^{\nu}\left(\lambda^2 - \frac{1}{\lambda}\right). \tag{47}$$

5.2 Region 2

In this region, collagen fibrils begin to tauten, with the number of fibrils tautening increasing with the stretch. This region is defined by $(1 + \mathrm{e}^{\tau}) \leqslant \lambda \leqslant \frac{(2+2\mathrm{e}^{\tau}+\mathrm{e}^{\rho})}{2}$, and the Cauchy stress is

$$\sigma_{zz} = \mathrm{e}^{\nu}\left(\lambda^2 - \frac{1}{\lambda}\right) + 4\mathrm{e}^{(\eta-2\rho)}\left(\frac{\lambda^2}{2} - (1+\mathrm{e}^{\tau})\lambda\log\left(\frac{\lambda}{1+\mathrm{e}^{\tau}}\right) - \frac{(1+\mathrm{e}^{\tau})^2}{2}\right). \tag{48}$$

5.3 Region 3

In this region, collagen fibrils continue to tauten but the number of fibrils tautening decreases with the stretch. This region is defined as $\frac{(2+2\mathrm{e}^{\tau}+\mathrm{e}^{\rho})}{2} < \lambda \leqslant (1 + \mathrm{e}^{\tau} + \mathrm{e}^{\rho})$, and the Cauchy stress is

$$\begin{aligned}\sigma_{zz} = \mathrm{e}^{\nu}\left(\lambda^2 - \frac{1}{\lambda}\right) + 4\mathrm{e}^{(\eta-2\rho)}\Bigg((1+\mathrm{e}^{\tau})\lambda\log(1+\mathrm{e}^{\tau}) - \frac{(1+\mathrm{e}^{\tau})^2}{2} - \frac{\lambda^2}{2} + (1+\mathrm{e}^{\tau}+\mathrm{e}^{\rho})\lambda\log(\lambda)\\ - (2+2\mathrm{e}^{\tau}+\mathrm{e}^{\rho})\lambda\log\left(\frac{2+2\mathrm{e}^{\tau}+\mathrm{e}^{\rho}}{2}\right) + \frac{(2+2\mathrm{e}^{\tau}+\mathrm{e}^{\rho})^2}{4}\Bigg).\end{aligned} \tag{49}$$

5.4 Region 4

In this region, every collagen fibril is taut. The region is defined as $(1 + \mathrm{e}^{\tau} + \mathrm{e}^{\rho}) < \lambda$, and the Cauchy stress is

$$\begin{aligned}\sigma_{zz} = \mathrm{e}^{\nu}\left(\lambda^2 - \frac{1}{\lambda}\right) + 4\mathrm{e}^{(\eta-2\rho)}\Bigg(-(2+2\mathrm{e}^{\tau}+\mathrm{e}^{\rho})\lambda\log\left(\frac{2+2\mathrm{e}^{\tau}+\mathrm{e}^{\rho}}{2}\right) + (1+\mathrm{e}^{\tau})\lambda\log(1+\mathrm{e}^{\tau})\\ + (1+\mathrm{e}^{\tau}+\mathrm{e}^{\rho})\lambda\log(1+\mathrm{e}^{\tau}+\mathrm{e}^{\rho}) - \frac{\mathrm{e}^{2\rho}}{4}\Bigg).\end{aligned} \tag{50}$$

6 Determining the parameters of the prior distribution

In order to determine the parameters, μ and σ^2, used in the log-normal priors of $(1-\phi)\mu$, ϕE, $a-1$, and $b-a$, and the normal priors of their logarithms, we estimated the values at which the cumulative probability density (CPD) of the prior reached 0.01 and 0.99 for each parameter and then used the quantile function to determine μ and σ^2. For the log-normal distribution, the quantile function is

$$q = \exp(\mu + \sqrt{2\sigma^2}\mathrm{erf}^{-1}(2p-1)), \tag{51}$$

where q is the value of the parameter, erf^{-1} represents the inverse error function, and p is the CPD. The list of values chosen for 0.01 and 0.99 cumulative density and the reasons for choosing them are listed in Table 1.

7 Additional RWM plots

As mentioned in the main paper, we also estimated parameter posteriors by fitting to the t5c and t6b data sets using the RWM algorithm. For the t5c data set, the estimated posteriors and the two-dimensional contour plots of the various joint distributions are given in Figure 5 for the untransformed parameters. The mean and 5σ confidence band of a set of 50,000 positions from the Markov chains, that is, parameter vectors, are also plotted in Figure 6. For the t6b data set, we also plotted the estimated parameter posteriors and two-dimensional contour plots of the joint distributions in Figure 7, and the means and 5σ confidence band of a subset of 50,000 parameter vectors from

Parameter	0.01 CPD	0.99 CPD	Reason
$(1-\phi)\mu$ (MPa)	0.001	10	**Lower**: motivated by the values of μ for tendon fascicles obtained by Purslow [3] **Higher**: inclusive upper bound.
ϕE (MPa)	3.072	13,600	**Lower**: inclusive lower bound using low estimates of $\phi = 0.096$ [4] and $E = 32$ MPa by [5]. **Higher**: inclusive upper bound using an estimate of $\phi = 0.85$ and $E = 16$ GPa given by [6] and [7], respectively.
$a - 1$	0.005	0.1	**Lower**: attempt to provide an inclusive lower bound. **Higher**: assumption that at least one fibril has tautened by the end of the stress-strain data we fit to.
$b - a$	0.005	0.15	**Lower**: attempt to provide an inclusive lower bound. **Higher**: attempt to provide an inclusive upper bound.

Table 1: A table of values used to calculate the mean and variance of the prior distributions of the ST model's parameters. In order to allow the posterior parameter space to be fully sampled in the RWM algorithm, the priors were designed to be inclusive of a wide range of parameter values.

the Markov chains in Figure 8. To create Figures 5 and 7, the samples from the Markov chains were thinned by a factor of ten, as they were for the higher-resolution data sets discussed in the main paper.

Comparing Figures 5—8 with their counterparts for the higher-resolution data shown in the main paper, the estimated parameter posteriors are generally broader and, in some cases, possess a long tail in one direction of the distribution, causing more probability mass to be located in the tail. Furthermore, the confidence bands of the estimated stress values from parameter vectors in the Markov chains are significantly wider, with the 'curves' being more angular than equivalent curves for the synthetic, SDFT, and CDET data sets due to the lack of data points we fit to. In order to ensure we sampled from the target distributions, we extended the burn-in phase to be 1 million simulations. Before we attempt to identify why these differences occur, we note that the data collected by Goh *et al.* were not intended to be used in the fitting of hyperelastic SEFs, but instead to study tendon behaviour for elastic and plastic deformation and, then, failure.

The lack of points to fit to likely causes the aforementioned differences in the posteriors for two main reasons. Firstly, it is harder to distinguish the regions of the SEF from one another when there are fewer points to fit to. The value of $(1-\phi)\mu$ is less important, in terms of the overall fit, when there are few data points in the toe region and collagen fibrils are active for nearly all data points. A wider range of values for $(1-\phi)\mu$ can be proposed and accepted, therefore. This has also been shown in the main paper with the high-resolution CDET data. Secondly, the posterior-predictive is dependent on the difference between the experimental and predicted stresses, and the acceptance probability κ is dependent on the ratio of the value of the posterior-predictive of the proposed parameter vector to that of the current position of the Markov chains. Fitting to fewer points means that differences in the value of the posterior-predictive will be less pronounced between close and relatively poor fits to data. Therefore, the prior ratio and the posterior-modification ratio have a greater effect on the calculation of κ. The latter ratio is dependent on the proposed value of ϕE, for instance. Consequently, large values of ϕE are proposed and accepted, as we see in Figures 5 and 7.

As mentioned previously, the posteriors of parameters such as ϕE and b are broad for these data sets with wide tails in certain directions. Consequently, the confidence bands, calculated from the predicted stresses of 50,000 positions of the Markov chains, are broader than for the high-resolution data. In contrast to the high-resolution h16 SDFT data and the synthetic data, some of the two-dimensional contour plots possess contour lines that are not elliptical, but instead are more complex in shape. This makes it harder for the RWM algorithm to propose enough parameter vectors that are accepted, which impacts the ability of the algorithm to run efficiently. However, the posteriors are generally smooth, which suggests that some level of convergence in the posteriors has been reached, and justifies the use of a longer burn-in phase. Additionally, all of the data points lie within the 5σ confidence band and close to the mean line, demonstrating the ability of the model to replicate experimental data.

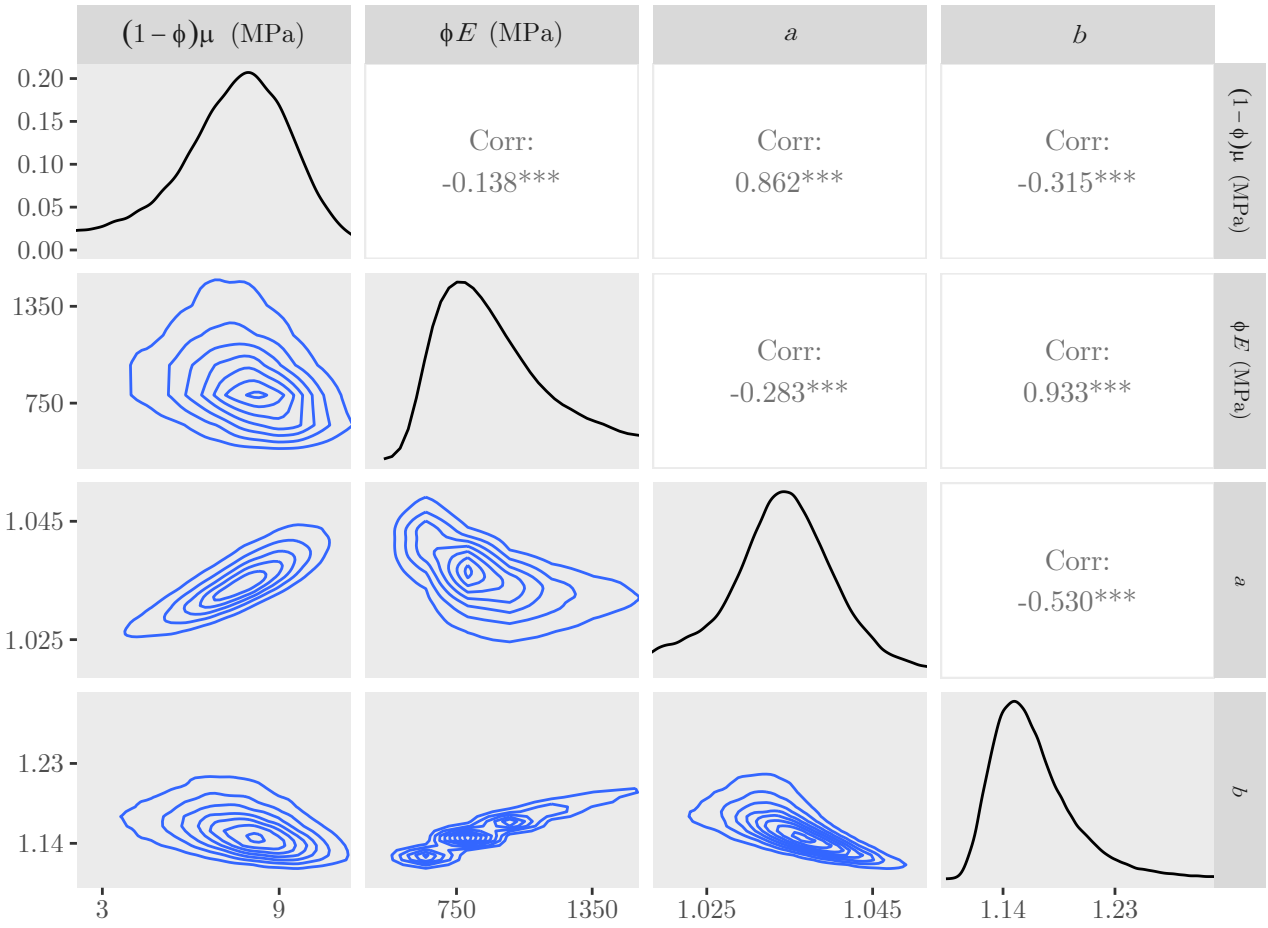

Figure 5: Estimated posteriors and contours of the joint distributions of the untransformed parameters for the fit to the t5c data.

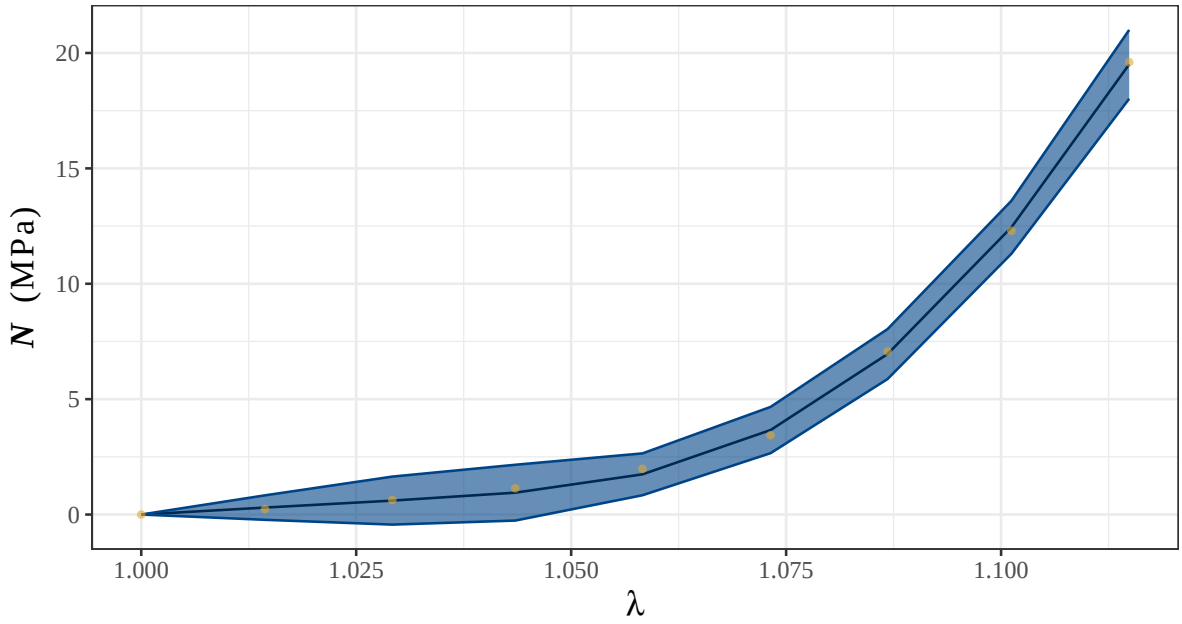

Figure 6: The mean (black) and 5σ confidence band (blue) of the fits to the t5c data (yellow dots).

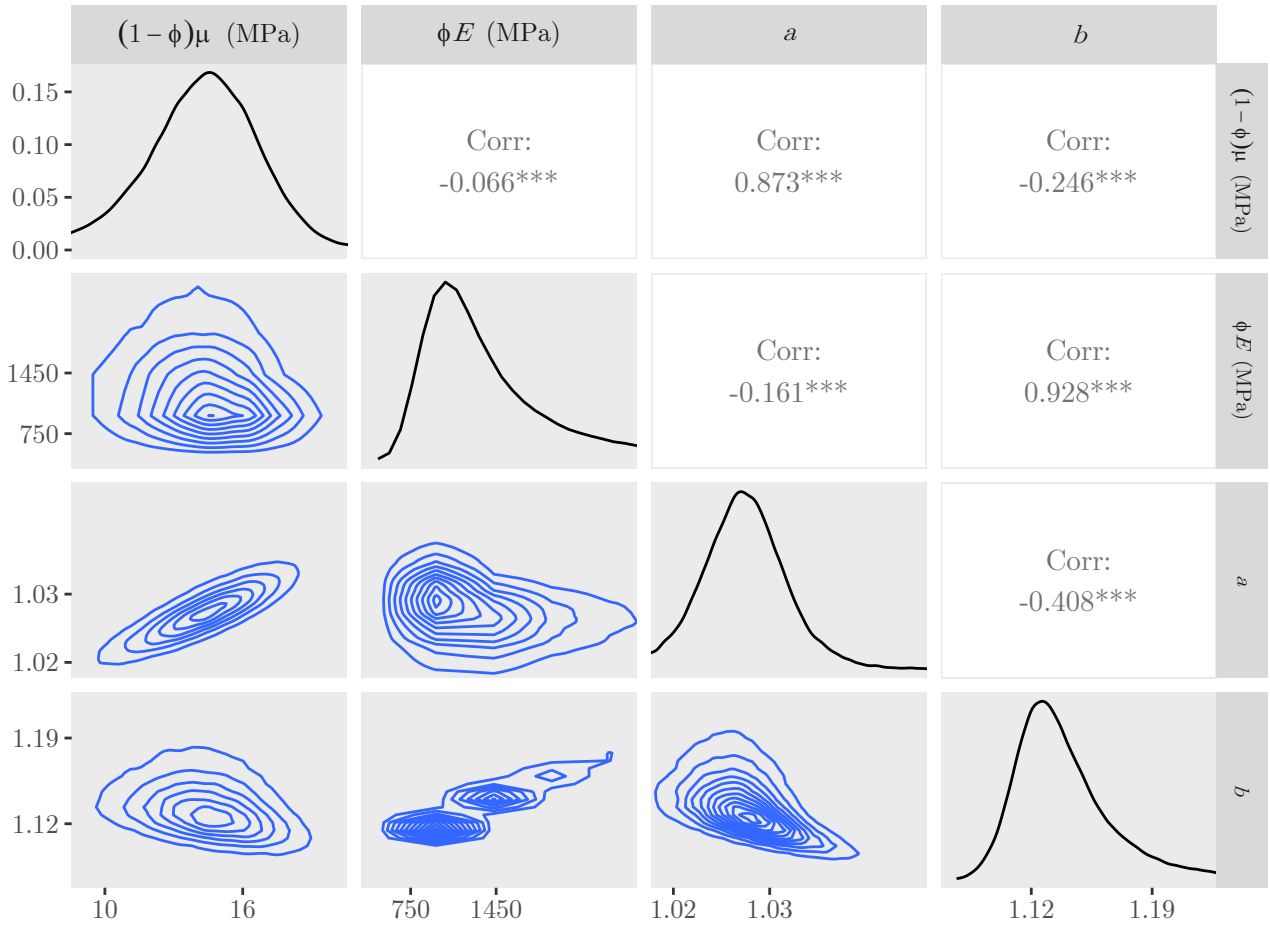

Figure 7: Estimated posteriors and contours of the joint distributions of the untransformed parameters for the fit to the t6b data.

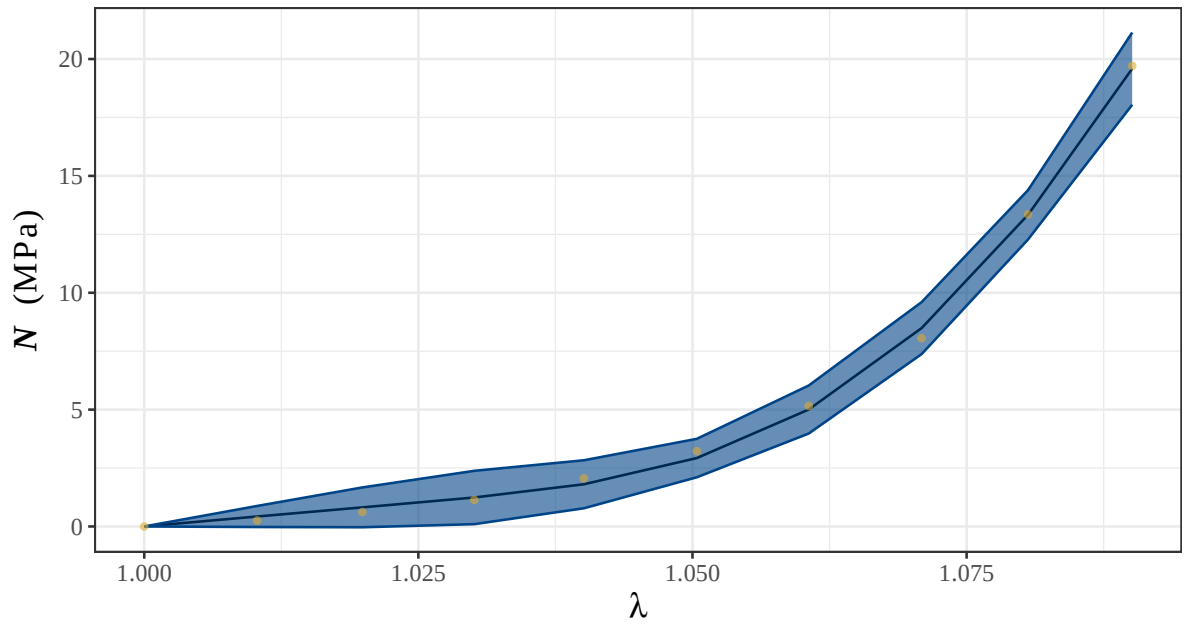

Figure 8: The mean (black) and 5σ confidence band (blue) of the fits to the t6b data (yellow dots).

8 RWM using the GT model

As mentioned in the main paper, we fit the GT model to the high-resolution SDFT data using the RWM algorithm. In this section, therefore, we detail how we adapted the RWM algorithm to the GT case. The GT model possesses five parameters: $(1-\phi)\mu$ (MPa), ϕE (MPa), a, c, and b. The additional parameter c is the modal recruitment stretch. For the GT model, we restrict the distribution parameters as follows: $1 < a < c < b$. As we did for the ST model, we transform the parameters so that the support of each parameter extends over the entire real axis, thereby increasing the efficiency of sampling in the RWM algorithm. Firstly, we replace a, c, and b with $a-1$, $c-a$, and $b-c$. Each of these parameters must be strictly greater than zero; therefore, we can take the logarithm of each quantity to extend its support over the entire real axis. We have

$$\boldsymbol{\theta}_{\mathrm{GT}} = \begin{pmatrix} \nu \\ \eta \\ \tau \\ \xi \\ \chi \end{pmatrix} = \begin{pmatrix} \log((1-\phi)\mu) \\ \log(\phi E) \\ \log(a-1) \\ \log(c-a) \\ \log(b-c) \end{pmatrix} = \mathrm{T}(\boldsymbol{\psi}_{\mathrm{GT}}), \tag{52}$$

With the set of parameters $\boldsymbol{\theta}_{\mathrm{GT}}$, the map-induced density becomes

$$\det D_{T^{-1}}(\boldsymbol{\theta}_{\mathrm{GT}}) = \exp(\nu+\eta+\tau+\xi+\chi), \tag{53}$$

$$\tilde{\pi}(\boldsymbol{\theta}_{\mathrm{GT}}) = \pi(T^{-1}(\boldsymbol{\theta}_{\mathrm{GT}})).\exp(\nu+\eta+\tau+\xi+\chi). \tag{54}$$

Finally, as we have introduced two new parameters, $c-a$ and $b-c$, we must define values that correspond to 0.01 and 0.99 of their CPD to calculate the mean and variance of their log-normal prior distributions. We chose the values of the 0.01 and 0.99 CPD thersholds for $c-a$ and $b-c$ to match those of the parameter $b-a$ shown in Table 1 (i.e. we set the 0.01 CPD threshold to be 0.005 and the 0.99 CPD threshold to be 0.15).

8.1 Transformation of the engineering stress

To use the GT model in the RWM algorithm, we must write the constitutive equation for the GT model in terms of the transformed parameters, ν, η, τ, ξ and χ. As in Section 5, we assume that the tendon sample studied undergoes a uniaxial stretch along the z-axis, which coincides with the orientation of the collagen fibrils. Furthermore, we assume traction-free boundary conditions on the lateral faces. The only non-zero component of the Cauchy stress is similar to (46), but with (21)–(24) replaced by (8)–(11). That is,

$$\sigma_{zz} = (1-\phi)\mu\left(\lambda^2 - \frac{1}{\lambda}\right) + \phi E(A(\lambda) + B(\lambda)\lambda + C(\lambda)\lambda^2 + D(\lambda)\lambda\log\lambda). \tag{55}$$

We can use (8)–(11) and (55) to write σ_{zz} explicitly in terms of λ and the transformed parameters for each region specified by the piecewise constants. As in Section 5, the following equations for σ_{zz} are divided by λ to find the corresponding expressions for the engineering stress.

8.2 Region 1

In this region, every collagen fibril is crimped and slack, as the stretch is less than the minimum recruitment stretch. Only the non-collagenous matrix contributes to the tendon's resistance to the deformation. In terms of the transformed parameters, this region is defined as $\lambda < 1 + \mathrm{e}^{\tau}$ and the Cauchy stress is

$$\sigma_{zz} = \mathrm{e}^{\nu}\left(\lambda^2 - \frac{1}{\lambda}\right). \tag{56}$$

8.3 Region 2

In this region, collagen fibrils begin to tauten, with the number of fibrils tautening increasing with the stretch. This is because the stretch is less than the modal recruitment stretch. This region is defined by $(1+\mathrm{e}^{\tau}) \leqslant \lambda \leqslant (1+\mathrm{e}^{\tau}+\mathrm{e}^{\xi})$, and the Cauchy stress is

$$\sigma_{zz} = \mathrm{e}^{\nu}\left(\lambda^2 - \frac{1}{\lambda}\right) + \frac{\mathrm{e}^{\eta}}{(\mathrm{e}^{\xi}+\mathrm{e}^{\chi})\mathrm{e}^{\xi}}\left(\lambda^2 - 2(1+\mathrm{e}^{\tau})\lambda\log\left(\frac{\lambda}{1+\mathrm{e}^{\tau}}\right) - (1+\mathrm{e}^{\tau})^2\right). \tag{57}$$

8.4 Region 3

In this region, collagen fibrils continue to tauten but the number of fibrils tautening decreases with the stretch. This is because the stretch is greater than the modal recruitment stretch. This region is defined as $(1+\mathrm{e}^{\tau}+\mathrm{e}^{\xi}) < \lambda \leqslant (1+\mathrm{e}^{\tau}+\mathrm{e}^{\xi}+\mathrm{e}^{\chi})$, and the Cauchy stress is

$$\begin{aligned}\sigma_{zz} = \mathrm{e}^{\nu}\left(\lambda^2-\frac{1}{\lambda}\right) &+ \frac{\mathrm{e}^{\eta}}{(\mathrm{e}^{\xi}+\mathrm{e}^{\chi})\mathrm{e}^{\xi}}[-(1+\mathrm{e}^{\tau})^2+2\lambda(1+\mathrm{e}^{\tau})\log(1+\mathrm{e}^{\tau})] \\ &+ \frac{\mathrm{e}^{\eta}}{\mathrm{e}^{\xi}\mathrm{e}^{\chi}}[(1+\mathrm{e}^{\tau}+\mathrm{e}^{\xi})^2-2\lambda(1+\mathrm{e}^{\tau}+\mathrm{e}^{\xi})\log(1+\mathrm{e}^{\tau}+\mathrm{e}^{\xi})] \\ &+ \frac{\mathrm{e}^{\eta}}{(\mathrm{e}^{\xi}+\mathrm{e}^{\chi})\mathrm{e}^{\chi}}[-\lambda^2+2\lambda(1+\mathrm{e}^{\tau}+\mathrm{e}^{\xi}+\mathrm{e}^{\chi})\log(\lambda)]. \end{aligned} \tag{58}$$

8.5 Region 4

In this region, every collagen fibril is taut, as the stretch is greater than the maximum recruitment stretch. The region is defined as $(1+\mathrm{e}^{\tau}+\mathrm{e}^{\xi}+\mathrm{e}^{\chi}) < \lambda$, and the Cauchy stress is

$$\begin{aligned}\sigma_{zz} = \mathrm{e}^{\nu}\left(\lambda^2-\frac{1}{\lambda}\right) - \mathrm{e}^{\eta} &+ \frac{\mathrm{e}^{\eta}[2\lambda(1+\mathrm{e}^{\tau})\log(1+\mathrm{e}^{\tau})]}{(\mathrm{e}^{\xi}+\mathrm{e}^{\chi})\mathrm{e}^{\xi}} - \frac{\mathrm{e}^{\eta}[2\lambda(1+\mathrm{e}^{\tau}+\mathrm{e}^{\xi})\log(1+\mathrm{e}^{\tau}+\mathrm{e}^{\xi})]}{\mathrm{e}^{\xi}\mathrm{e}^{\chi}} \\ &+ \frac{\mathrm{e}^{\eta}[2\lambda(1+\mathrm{e}^{\tau}+\mathrm{e}^{\xi}+\mathrm{e}^{\chi})\log(1+\mathrm{e}^{\tau}+\mathrm{e}^{\xi}+\mathrm{e}^{\chi})]}{(\mathrm{e}^{\xi}+\mathrm{e}^{\chi})\mathrm{e}^{\chi}}. \end{aligned} \tag{59}$$

References

[1] Shearer T. A new strain energy function for the hyperelastic modelling of ligaments and tendons based on fascicle microstructure. Journal of biomechanics. 2015;48(2):290-7.

[2] Rynn JA, Cotter SL, Powell CE, Wright L. Surrogate accelerated Bayesian inversion for the determination of the thermal diffusivity of a material. Metrologia. 2019;56(1):015018.

[3] Purslow PP. The shear modulus of connections between tendon fascicles. In: 2009 IEEE Toronto International Conference Science and Technology for Humanity (TIC-STH). IEEE; 2009. p. 134-6.

[4] Silver FH, Seehra GP, Freeman JW, DeVore D. Viscoelastic properties of young and old human dermis: a proposed molecular mechanism for elastic energy storage in collagen and elastin. Journal of Applied Polymer Science. 2002;86(8):1978-85.

[5] Graham JS, Vomund AN, Phillips CL, Grandbois M. Structural changes in human type I collagen fibrils investigated by force spectroscopy. Experimental cell research. 2004;299(2):335-42.

[6] Goh KL, Holmes DF, Lu HY, Richardson S, Kadler KE, Purslow PP, et al. Ageing Changes in the Tensile Properties of Tendons: Influence of Collagen Fibril Volume Fraction. Journal of Biomechanical Engineering. 2008 03;130(2). 021011. Available from: `https://doi.org/10.1115/1.2898732`.

[7] Gautieri A, Vesentini S, Redaelli A, Ballarini R. Modeling and measuring visco-elastic properties: From collagen molecules to collagen fibrils. International Journal of Non-Linear Mechanics. 2013;56:25-33.